Pharm Res (2015) 32:1947–1956
DOI 10.1007/s11095-014-1588-8

RESEARCH PAPER

# Polypeptide-based Micelles for Delivery of Irinotecan: Physicochemical and *In vivo* Characterization

Thiruganesh Ramasamy • Ju Yeon Choi • Hyuk Jun Cho • Subbaih Kandasamy Umadevi • Beom Soo Shin • Han-Gon Choi • Chul Soon Yong • Jong Oh Kim

Received: 13 August 2014 / Accepted: 24 November 2014 / Published online: 4 December 2014


## ABSTRACT

***Purpose*** Irinotecan (IRI) is a broad spectrum chemotherapeutic agent used individually or in combination to treat multiple malignancies. Present study aimed at developing polypeptide-based block ionomer complex (BIC) micelles to improve the pharmacokinetic and antitumor response of IRI.

***Methods*** Irinotecan-loaded BIC micelles (IRI-BIC) was prepared and evaluated in terms of various physicochemical and biological parameters including size, shape, release, cytotoxicity, and pharmacokinetic analysis. *In vivo* antitumor efficacy was investigated in SCC-7 bearing xenograft tumor model.

***Results*** IRI was successfully incorporated into the ionic cores of poly(ethylene glycol)-*b*-poly(aspartic acid) (PEG-*b*-PAA) with a high drug loading capacity (~80%). The electrostatically assembled BIC micelles were nanosized (~50 nm) with uniform size distribution pattern (PDI~0.1). The BIC micelles exhibited pH-sensitiveness with limited release of IRI at physiological conditions and significantly enhanced the release rate at acidic conditions, making it an ideal delivery system for tumor targeting. The IRI-BIC showed a dose-dependent cytotoxicity in SCC-7 and A-549 cancer cell lines. Pharmacokinetic studies clearly showed that BIC micelles improved the IRI blood circulation time and decreased its elimination rate constant, while that of free IRI, rapidly eliminated from the central compartment. Moreover, IRI-BIC showed superior therapeutic performance with no toxicity in BALB/c nude xenograft mice. The micelle treated group showed an inhibition rate of ~66% compared to free IRI treated group.

***Conclusions*** Taken together, BIC micelles could be a potentially useful nanovehicle with promising applicability in systemic tumor treatment.

**KEY WORDS** anticancer · block ionomer complex · irinotecan · polypeptide · self-assembly

## ABBREVIATIONS

| | |
|---|---|
| ABS | Acetate buffered saline |
| AUC | The area under the drug concentration–time curve from 0 to 24 h |
| BIC | Block ionomer complex |
| Cl | Clearance |
| $C_{max}$ | The peak concentration of drug |
| DLS | Dynamic light scattering |
| EPR | Enhanced permeation and retention effect |
| FT-IR | Fourier transform infrared spectroscopy |
| IRI | Irinotecan |
| IRI-BIC | Irinotecan-loaded BIC |
| $K_{el}$ | Elimination rate constant |
| MRT | Mean retention time |
| PBS | Phosphate buffered saline |

**Electronic supplementary material** The online version of this article (doi:10.1007/s11095-014-1588-8) contains supplementary material, which is available to authorized users.

T. Ramasamy • J. Y. Choi • H. J. Cho • C. S. Yong (✉) • J. O. Kim (✉)
College of Pharmacy, Yeungnam University, 214-1, Dae-dong
Gyeongsan 712-749, South Korea
e-mail: csyong@ynu.ac.kr
e-mail: jongohkim@yu.ac.kr

S. K. Umadevi
St. Paul's College of Pharmacy, Osmania University, Hyderabad, Andhra Pradesh, India

B. S. Shin
College of Pharmacy, Catholic University of Daegu, Gyeongsan 712-702 South Korea

H.-G. Choi
College of Pharmacy, Institute of Pharmaceutical Science and Technology
Hanyang University, 55, Hanyangdaehak-ro, Sangnok-gu
Ansan 426-791, South Korea

| | |
|---|---|
| PDI | Polydispersity index |
| PEG-*b*-PAA | Poly(ethylene glycol)-*b*-poly(aspartic acid) |
| $t_{1/2}$ | Half-life |
| TEM | Transmission electron microscope |
| $T_{max}$ | The time to reach the peak concentration |
| $V_{ss}$ | Volume of distribution |
| XRD | X-ray diffractometer |

## INTRODUCTION

Irinotecan (IRI) is a highly potent anticancer agent that exerts its effect by inhibition of topoisomerase I, resulting in inhibition of DNA replication and transcription [1–3]. IRI is effective against a wide range of malignancies including lymphoma, gastric, colorectal, cervical, ovarian, and lung cancer [4]. Despite its *in vitro* effects, systemic delivery of IRI is hampered by severe side effects such as cholinergic syndrome and other adverse effects [5, 6]. In an effect to overcome these issues, various drug delivery systems including liposomes, dendrimers, and polymer conjugates have been extensively investigated [7, 8]. However, serious drawbacks such as low therapeutic efficacy, *in vivo* instability, premature burst release, and low drug loading have limited its clinical success [9, 10]. In particular, low drug loading would require repeated administration of a large quantity of carrier/drug, while *in vivo* instability would cause rapid clearance of the drug from the blood circulation. Therefore, there is an unmet need for development of an efficient delivery system to not only improve the therapeutic efficiency but also minimize drug-related adverse effects.

Polymer-based nanoparticulate drug delivery systems have attracted significant attention of researchers in recent years. Specifically, polymeric micelles based on the self-assembly of block copolymers is considered as a potential vehicle for delivery of anti-cancer drugs [11]. The nanosize, narrow size distribution, core-shell architecture, and high drug loading are some of the characteristics features of polymeric micelles [12, 13]. In addition, these carriers are believed to augment enhanced permeation and retention (EPR) effect in tumors by prolonging the blood circulation time in the body [14]. According to previous reports, accumulation of micellar carriers in tumor interstitial can lead to significant tumor regression with negligible intrinsic toxicity. In particular, the presence of a poly(ethylene glycol) (PEG) shell on nanoparticles prevents interactions with serum proteins, and evades the reticuloendothelial system (RES) [15, 16].

Nanofabrication of polymeric micelles has been significantly advanced by the introduction of charge-driven block copolymers with water soluble ionic and nonionic segments (ionomers) [11]. Such block ionomers electrostatically interact with the oppositely charged moieties, resulting in block ionomer complex (BIC) micelles. These micelles are formed spontaneously due to the charge neutralization, formation of hydrophobic domain, and segregation in the aqueous media [17]. The core of the micelles serves as a reservoir that accommodates the therapeutic species *via* various physical forces [18, 19]. The simplicity of carrier fabrication and avoidance of any harsh preparatory steps/chemicals/surfactants that may cause systemic toxicity are two important features of such BIC micelles [17]. This approach has been used to incorporate various charged species including small molecules, proteins, and nucleic acids. For example, doxorubicin was efficiently loaded into the polyanionic core of poly(ethylene oxide)-*b*-poly(methacrylic acid) and Pluronic P85-*b*-poly(acrylic acid) [17, 20, 21].

In the current study, we further explored this approach for the systemic delivery of cationic IRI, a weak base in physiological conditions. Electrostatic interaction of IRI with poly(ethylene glycol)-*b*-poly(aspartic acid) (PEG-*b*-PAA) resulted in formation of stable BIC micelles. In this complex, the amine group of IRI electrostatically binds with the carboxylate group of block copolymers in a highly cooperative manner. IRI-loaded BIC (IRI-BIC) remarkably prolonged the blood circulation time of drug with substantial tumor regression profile. The successful formulation of IRI-BIC was examined in terms of physicochemical properties, loading efficacy, and release study. *In vitro* cytotoxicity assays were performed on two different cell lines, SCC-7 and A-549 and *in vivo* anti-tumor activity was investigated on a xenograft tumor model.

## MATERIALS AND METHODS

### Materials

PEG-*b*-PAA ($M_w/M_n = 1.20$, MW = 12000) was purchased from Alamanda Polymers, Inc. (Huntsville, AL, USA). The block lengths were 113 and 50 repeating units for PEG and PAA, respectively. IRI was a generous gift from Hanmi Pharmaceuticals, Co. Ltd. (Hwaseong, South Korea). The SCC-7 and A-549 cell lines were originally obtained from the Korean Cell Bank (Seoul, South Korea). All other chemicals were of reagent grade and were used without further purification.

### Preparation of Irinotecan-Loaded BIC Micelles

The irinotecan-loaded BIC micelle (IRI-BIC) was formulated by simple addition method as reported previously [17, 22]. Briefly, aqueous drug solution and PEG-*b*-PAA copolymer solutions were prepared and mixed at various weight ratios of the drug to polymer, followed by vortex for 30 min at room temperature. The pH of aqueous solutions was maintained at 7 to ensure maximum physical interactions. Unbound drugs were removed by ultrafiltration using Amicon YM-10

centrifugal filter devices (MWCO 10000 Da, Millipore). The concentrations of IRI in filtrates and in the micelles were determined by HPLC method (Hitachi, Tokyo, Japan).

### Micelles Characterization

The average particle size, polydispersity index (PDI), and ζ-potential were measured by dynamic light scattering (DLS) method (Zeta Sizer Nano ZS; Malvern Instruments, Worcestershire, UK). Measurements were performed at a fixed scattering angle of 90° at a wavelength of 635 nm and at room temperature (25°C). ζ-potential was examined using the Smoluchowski equation. Overall, all measurements were determined using the manufacturer's software (NanoDTS software, version 6.34). All experiments were performed at least three times.

### Loading Capacity and Loading Efficiency

The loading capacity (LC) and loading efficiency (LE) were determined by centrifugal ultrafiltration method. For this purpose, free drug and drug-loaded micellar solutions were separated by high speed ultracentrifugation using an Amicon centrifugal filter device (MWCO 10000 Da, Millipore). The filtrate containing unbound drugs was determined by HPLC method. The mobile phase (water:acetonitrile:methanol, 50:25:25, pH 3.5) was run at 1 mL/min with an absorbance of 254 nm. The LC% and LE% were calculated using the following equations:

$$\textit{Loading capacity}\ (\%) = \left(\mathrm{IRI_{total}} - \mathrm{IRI_{unbound}}\right) / \left(\mathrm{Micelle_{total}}\right) \times 100$$

$$\textit{Loading efficiency}\ (\%) = \left(\mathrm{IRI_{total}} - \mathrm{IRI_{unbound}}\right) / \left(\mathrm{IRI_{total}}\right) \times 100$$

where $\mathrm{IRI_{total}}$, $\mathrm{IRI_{unbound}}$, and $\mathrm{Micelle_{total}}$ are the total amount of IRI added, unbound IRI, and micelles, respectively.

### Physical Characterization

Fourier transform infrared spectroscopy (FT-IR) spectra of PEG-*b*-PAA, IRI, and IRI-BIC were recorded using a Thermo Scientific Nicolet Nexus 670 FT-IR Spectrometer and Smart iTR with a diamond window (Thermo Fisher Scientific Inc., Waltham, MA): 5 mg of lyophilized samples were used to record the FTIR spectra. The spectrum was set in the range between 600 and 4000 $cm^{-1}$ at a resolution of 4 $cm^{-1}$ with 32 scans per sample.

Powder X-Ray analysis was performed using an X-ray diffractometer (X'Pert PRO MPD diffractometer, Almelo, the Netherlands) with a copper anode (Cu Kα radiation) as a source of radiation. The XRD patterns were recorded at an optimum voltage of 40 kV, current of 30 mA radiation, and a scanning rate of 0.013 $min^{-1}$ over a 2θ (diffraction angle) range between 10 and 60°C at room temperature.

### Morphological Analysis

The shape and surface morphology of IRI-BIC was examined using a transmission electron microscope (TEM; H-7600, Hitachi, Tokyo, Japan) at an accelerating voltage of 100 kV. Briefly, a drop of formulation was placed on a carbon-coated copper grid (300 mesh) and allowed to settle for 5 min. The excess dispersions were removed, and 2% phosphotungstic acid solution was added as a negative staining agent. The samples were air-dried under infrared radiation for 10 min.

### *In vitro* Release Study

The *in vitro* release of IRI from micelles was measured in phosphate buffered saline (PBS, pH 7.4, 0.14 M NaCl) and acetate buffered saline (pH 5.0, 0.14 M NaCl) at 37°C. A dialysis bag of low molecular weight cut off (Spectra/Por; 3500 Da cutoff) was selected for performance of the release experiments. Briefly, 1 mL micellar dispersions were placed in the dialysis bag which was in turn imbibed in 25 mL respective release media in screw-capped tubes. The tubes were placed in an orbital shaker bath (100 rpm, 37°C) and samples were collected at predetermined time intervals. Sink conditions were maintained throughout the release experiments. The cumulative percentage of drug release was determined using the HPLC method as described above.

### *In vitro* Cytotoxicity

SCC-7 squamous carcinoma cells and A-549 small lung cancer cells were grown in RPMI 1640 medium supplemented with 10% (*v*/*v*) fetal bovine serum (FBS) in the presence of penicillin and streptomycin (100 U/mL and 0.1 mg/mL, respectively). The cells were maintained under ambient conditions (37°C containing 5% $CO_2$) in a T-75 flask and periodically subcultured. The *in vitro* cell viability assay was performed as reported previously [23]. Briefly, respective cells were seeded in 96-well microtiter plates at a density of $1 \times 10^4$ cells/well and incubated for 24 h to allow cell adhesion. The cells were treated with free IRI and IRI-BIC at concentrations ranging from 1 to 100 μg/mL followed by incubation for an additional 24 h. The next day, old media was replenished with

fresh media and further incubated for 72 h to allow expansion of the cells; 100 μL of MTT solution (1.25 mg/mL) was added to each of the 96-well, followed by incubation for 3–4 h in a dark place at 37°C. Finally, DMSO was added to dissolve the formazan crystals and the absorbance was read at 570 nm using a microplate reader (Multiskan EX, Thermo scientific, USA). Cell viability was calculated using the following equations:

$$\text{Cell viability } (\%) = \left(\text{INT}_{sample}/\text{INT}_{control}\right) \times 100$$

where $\text{INT}_{sample}$ is the colorimetric intensity of sample cells and $\text{INT}_{control}$ is the absorbance of control cells. $IC_{50}$ was calculated using GraphPad Prism software (Graphpad, San Diego, California), which is the concentration of drug required to kill 50% of viable cells.

## Pharmacokinetic Study

### *Drug Administration and Blood Sample Analysis*

The pharmacokinetic study was carried out in male Sprague Dawley rats (average weight 250 ± 5 g; 7 weeks old). Rats were caged in a clean and temperature/humidity controlled ambient environment with a 12 h dark–light circle, and given good humane care with free access to food and water throughout the housing. The study protocols were approved by the Institutional Animal Ethical Committee, Yeungnam University, South Korea in accordance with the national guidelines.

The rats were divided into two experimental groups with six rats in each group. They were fasted for 12 h before the experiment, but were given free access to water. The rats were anesthetized and cannulated in the right femoral artery for withdrawal of the blood samples, while the left femoral vein was cannulated in order to administer the respective formulations. Following drug administration, blood samples (250 μl) were collected at predetermined time intervals (0.25, 0.5, 1, 2, 4, 6, 8, 10, 12, and 24 h). The samples were immediately mixed with heparin (10 μL, prepared in 0.9% NaCL), centrifuged (Eppendorf, Hauppauge, NY, USA) at 13,000 rpm for 10 min, and stored at −80°C until further analysis.

The frozen plasma samples were thawed, 150 μL of sample was mixed with 150 μL of acetonitrile and vortexed for 30 min to precipitate interfering proteins. The sample was then centrifuged (13,000 rpm for 10 min) and supernatant was separated carefully leaving aside the pellet. The supernatant was evaporated in a vacuum dryer (Modul 3180C, Buchon, South Korea) and reconstituted with mobile phase; 20 μL of this reconstituted solution was injected into the HPLC column. The mobile phase consisted of water:acetonitrile:methanol (65:17.5:17.5) maintained at pH 3.5. The HPLC system consisted of a pump (Model L2100), an autosampler (Model L2200), and an ultraviolet detector (Model L2420). A $C_{18}$ analytic column (Inertsil ODS3: 0.5 μm, 15 cm × 0.46 cm,GL Sciences Inc., Japan) was used. The flow rate was maintained at 1 ml/min and effluent was monitored at 254 nm. The HPLC method was validated over the concentration range of 0.05 to 10 μg/ml. All standard curves showed excellent linearity with $R^2 = 0.9999$. The inter-day and intra-day precision RSD value was less than 7.2% while inter- and intra-day accuracy were more than 97%.

### *Pharmacokinetic Parameters*

The area under the drug concentration–time curve from 0 to 24 h (AUC), elimination rate constant ($K_{el}$), half-life ($t_{1/2}$), mean retention time (MRT), clearance (Cl), and volume of distribution ($V_{ss}$) were calculated using a non-compartmental analysis (WinNonlin; professional edition, version 2.1; Pharsight Co., MountainView, CA, USA). The peak concentration of drug ($C_{max}$) and the time to reach the peak concentration ($T_{max}$) were obtained directly from the plasma *versus* time profile. Levels of statistical significance ($p < 0.05$) were assessed using an ANOVA test. All data were expressed as the mean ± SD.

### *In vivo* Antitumor Study

A tumor xenograft model was prepared from 6-week old female BALB/c nude mice. For development of tumors, SCC-7 cells were cultivated, harvested, and implanted subcutaneously ($5 \times 10^6$ cells) into the right flank of mice. The mice were given good humane care and housed under ambient conditions, as described previously. Mice were assigned to three experimental groups, control (untreated), free IRI, and IRI-BIC at a dose of 5 mg/kg. The treatment regimen was started approximately 8 days after cell injection when the tumor volume reached 100–150 $mm^3$. The mice were injected *via* tail vein with respective formulations every 3 days for a total of four cycles. Tumor volume ($mm^3$) was measured using a vernier caliper and calculated using the following formula: $V(mm^3) = A(mm) \times B(mm)^2/2$, where A is the longest diameter and B is the shortest/widest diameter of the tumor. Body weight index was also monitored throughout the study period. At the end of the experiment, mice were sacrificed according to the institutional ethical guidelines. Tumors were surgically removed and weighed individually.

## RESULTS AND DISCUSSION

## Preparation of IRI-Loaded BIC Micelles

Irinotecan-loaded BIC micelles, IRI-BIC was prepared by the self-assembly of cationic drug into polyanionic cores. IRI, a

cationic drug electrostatically interacts with the PAA chain of PEG-*b*-PAA block copolymer, a weak base at the physiological pH, to form a core-shell nanoparticle with a hydrophobic core [11]. Specifically, the amine group of IRI interacted physically with the carboxylate group of PEG-*b*-PAA *via* electrostatic interactions. pH 7 was selected, at which pH sensitive polymer block remains in a highly ionized state, giving it maximum negative charge [22]. As seen in Fig. 1a, hydrodynamic particle size of IRI-BIC showed a consistent decrease for the increase in the weight ratio of IRI to PEG-*b*-PAA. The difference in size of the micelles at varied weight ratios of drug to polymer could be related to hydrophobicity of core, which could be due to the gradual neutralization of PAA segment in micelles with the stacking interaction of IRI [17]. Consistent with the decrease in particle size, surface charge gradually decreased with the increase in weight ratio of IRI (Figure S1). The final surface charge of optimized polymeric micelles was ~1.7 mV, indicating that at higher weight ratio, neutralization process is complete. Based on the results, it appears that IRI immobilzation

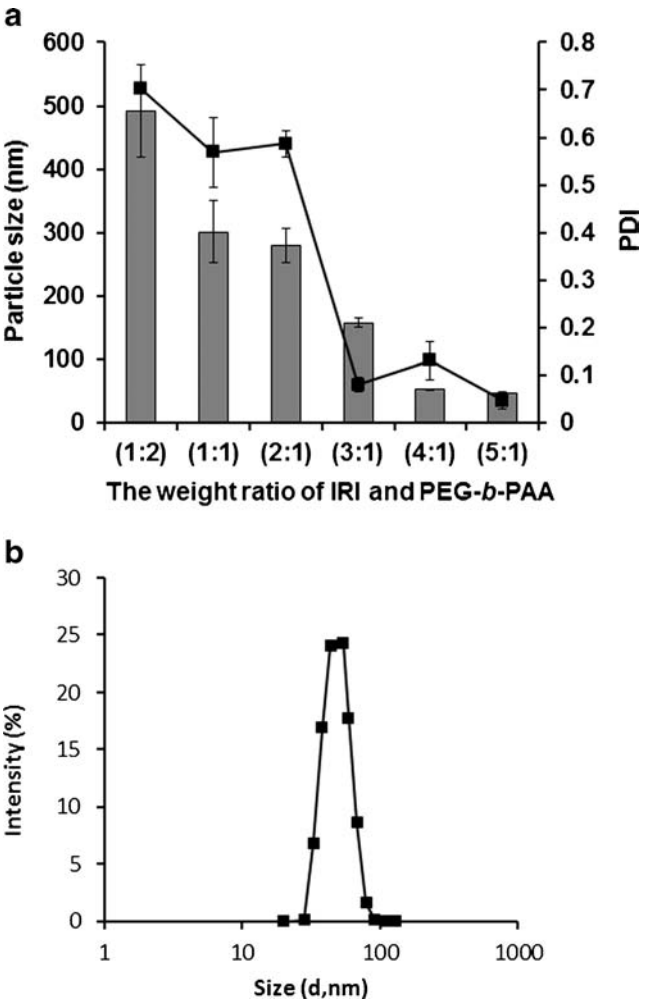


**Fig. 1** (**a**) Hydrodynamic size and polydispersity index of IRI-BIC at pH 7 as a function of weight ratio of IRI to PEG-*b*-PAA. (**b**) Particle size distribution of IRI-BIC prepared at weight ratio of 5:1.

was almost complete at a higher weight ratio (5:1), which resulted in a relatively hydrophobic core. At this ratio, high hydrophobicity and PEG shell possess sufficient steric repulsive power to maintain dispersion stability. It is noteworthy that IRI-BIC maintained good colloidal stability for aqueous dilution up to 20-fold (Figure S2) and also showed good storage stability up to two months without any obvious sign of precipitation or aggregation (Figure S3). This could be due to the presence of a hydrophilic PEG shell that minimizes the interfacial free energy and thereby inhibit interaction between particles.

Consistent with the particle size, polydispersity index of micelles also showed a considerable decrease for the increase in the weight ratio of IRI. Dispersion homogeneity of around 0.2 is regarded as uniform distribution of particles [24]. As seen, the PDI was less than < 0.1 at the optimized weight ratio of drug to polymer, indicating a relatively narrow size distribution of IRI-BIC. Typical size distribution profile of IRI-BIC (5:1) is presented in Fig. 1b, showing a unimodal size distribution. In general, a nanosized particle (50–100 nm) with uniform size distribution prolongs the blood circulation time of administered drug and increases the prospect of effective tumor targeting *via* EPR effect.

## Morphological Analysis

TEM image further confirmed the presence of nanosized micellar particles in the dried state. The strong electrostatic interaction between IRI and block copolymer was clearly visible in the microscopic imaging. Although a core-shell morphology was not observed, the particles were distinctly spherical in shape and largely presented a mono-dispersed pattern (Fig. 2). The darker core might be attributed to high electron density and higher packing density. The particle sizes were around ~40–50 nm, smaller than indicated in the DLS observation. The slight discrepancy in size from TEM and DLS data was ascribed to the fact that DLS gives a statistical mean particle size and distribution in the hydrated state, while TEM shows more qualitative localized viewing in a dried state.

## Drug Loading

Owing to the progressive neutralization of the polyionic segment, IRI-BIC showed high payload capacity (Fig. 3). Regardless of size, it showed good drug loading capacity even at lower weight ratio of drug to polymer. Such a high payload would decrease the frequency and overall quantity of drug loaded-carrier to be administered, to help improve the overall therapeutic efficiency.

## Physical Characterizations

FT-IR spectrum is used to evaluate the physical or chemical interaction between IRI and PEG-*b*-PAA. As shown in

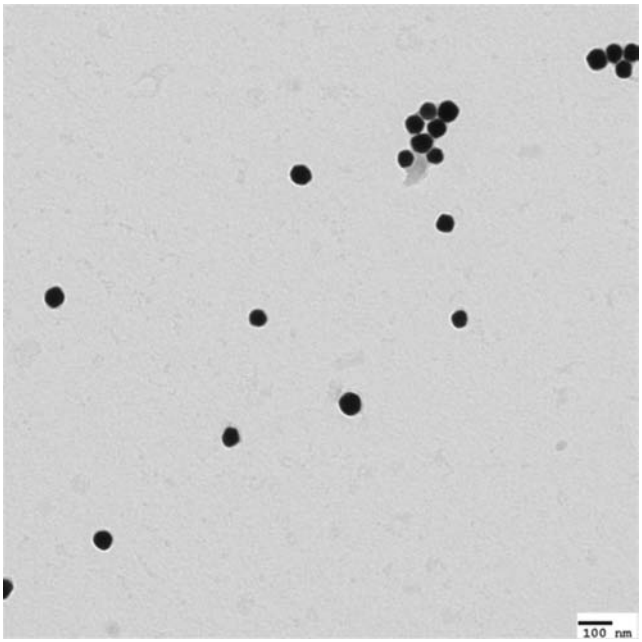


**Fig. 2** TEM image of IRI-BIC. IRI-BIC was prepared at a weight ratio of 5:1.

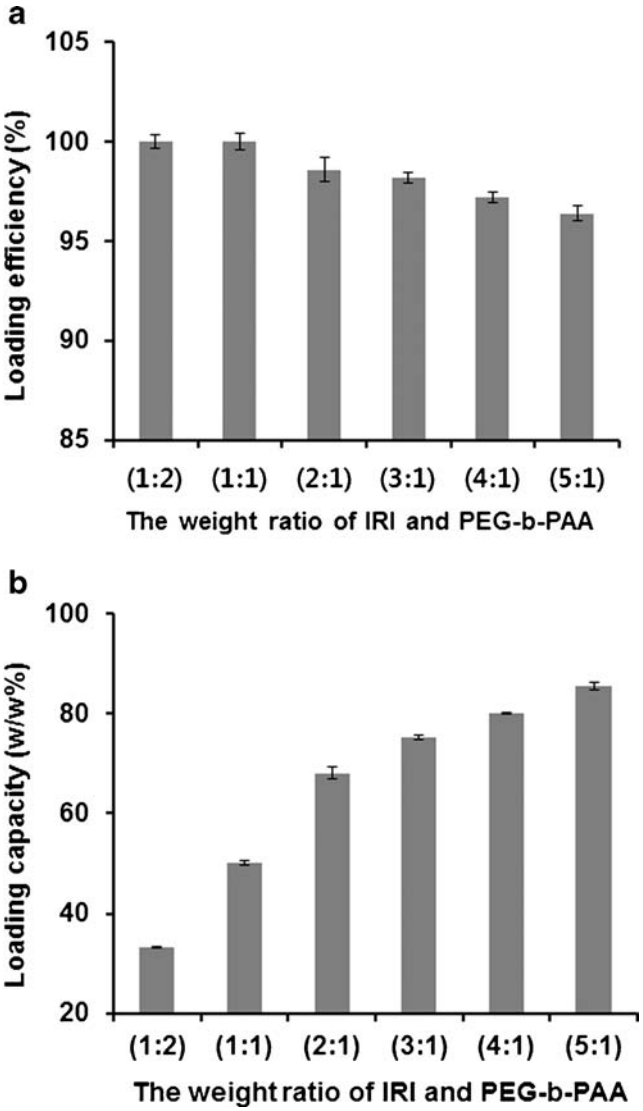


**Fig. 3** Loading efficiency and loading capacity of IRI-BIC as a function of weight ratio of drug to polymer.

Fig. 4a, IRI possessed multiple functional groups with C=O absorption band appeared in the region between 1870 and 1540 $cm^{-1}$ [25]. Specifically, the band at 1746 and 1715 $cm^{-1}$ is attributable to the stretching vibrations of carbonyl group (C=O) and its attachment to the quinolone component. The band at 1657 $cm^{-1}$ is assigned to the carbonyl group of the pyridone moiety. Most importantly, band at ~3350 $cm^{-1}$ is attributable to –NH vibration/stretching. Similarly, PEG-*b*-PAA block showed characteristic peaks at 1597 $cm^{-1}$ and 1403 $cm^{-1}$ corresponding to $COO^-$ groups of asymmetrical and symmetrical geometry, respectively. This COO- group will electrostatically interact with the protonated amine/amide group of IRI [26]. Moreover, broad spectrum at 3380 $cm^{-1}$ is assigned to $OH^-$ group that would be responsible for inter/intramolecular hydrogen bonding. Shift in the intensity of FT-IR spectrum would indicate the physicochemical interaction between the ionic blocks. As seen, the intensity of C=O stretching absorption bands in IRI showed a marked decrease, indicating a typical intermolecular and intramolecular hydrogen bonding with the PAA segment [27], while –NH absorption bands at ~3350 $cm^{-1}$ were shifted by some margin and the bands broadened, indicating the electrostatic interaction of IRI with the carboxylate group of PEG-*b*-PAA block. In addition, hydroxyl stretching vibrations at ~3364 $cm^{-1}$ also broadened, indicating the strengthening of hydrogen bonds [28].

XRD patterns of free IRI and IRI-BIC are shown in Fig. 4b. As can be seen, XRD diffractograms of IRI showed numerous sharp and intense peaks at various 2θ scattered angles reflecting its high crystalline nature. However, complete absence of such characteristic peaks suggests the incorporation of drug in the amorphous form. These observations clearly suggest that the drug is molecularly dispersed with the polymers. This is important from the point of view of stability, since the amorphous nature of drug prevents the Ostwald ripening phenomenon leading to a stable NP dispersion [29].

### *In vitro* Release Study

The drug release study was performed in phosphate-buffered saline (pH 7.4) and acetate-buffered saline (pH 5.0) by dialysis method. As shown in Fig. 5, IRI was gradually released with no distinct burst release phenomenon. Approximately ~40% of drug was released by 8 h, followed by a sustained release of drug up to 24 h of the study period. The faster release during the beginning of the study might be attributed to dissociation

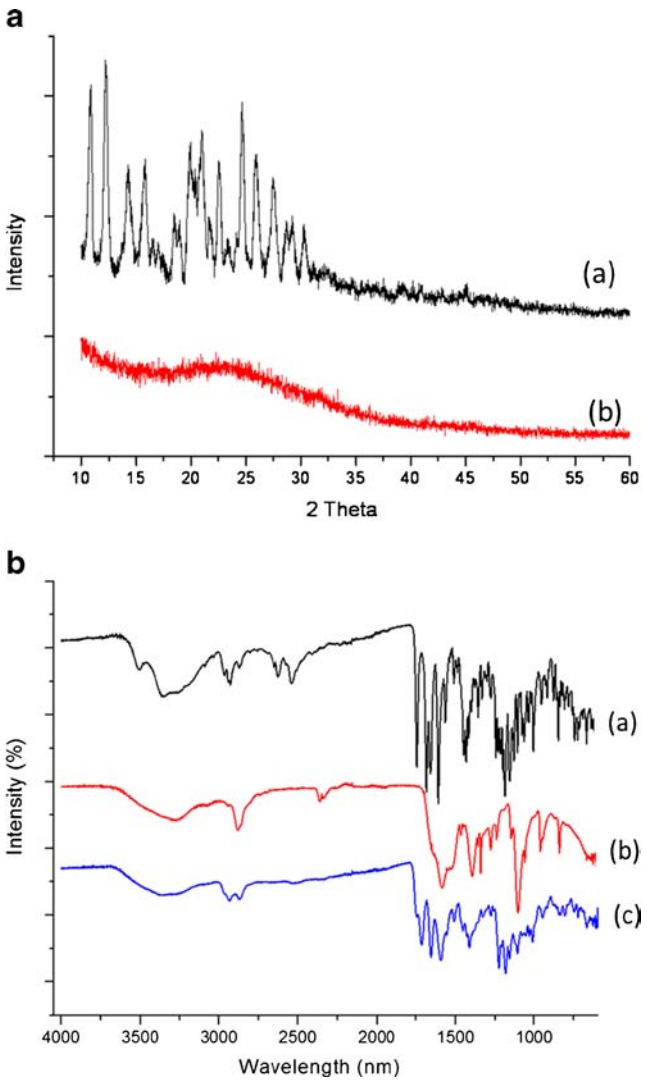


**Fig. 4** (**a**) XRD patterns of free IRI and IRI-BIC. (**b**) FTIR spectra of (*a*) IRI, (*b*) PEG-*b*-PAA, and (*c*) IRI-BIC.

of IRI from the block copolymer due to the presence of salt. It has been already reported that presence of a low molecular weight salt like NaCl would destabilize the salt bonds of BIC micelles [30]. Nevertheless, the ability of BIC micelles to provide a sustained release profile means a prolonged circulation in the physiological conditions of the body. In addition, we performed additional experiments in the ABS media to mimic the acidic environment of tumor. As cancer cells develop more acidic conditions, a delivery system with a lower release profile in the physiological environment and a distinctly higher release rate in the tumor environment would be an invaluable approach in cancer targeting. Ideally, a delivery system should be more specific to target and kill cancer cells. Previously, many researchers exploited the pH difference between normal cells and cancer cells by working on various drug delivery systems [31]. In the current study, we observed a remarkably higher release profile in acidic pH conditions. The accelerated release rate in acidic conditions may be attributed to protonation of the carboxylate group of the PAA segment of PEG-*b*-PAA copolymer within micelles [22]. Moreover, we have observed the release pattern in the presence of albumin (1%) (Figure S4). The release of IRI was slightly faster in the presence of albumin, but it was not significant. The relatively higher drug release was attributed to the interaction of albumin with the electrostatically assembled BIC micelles. The results clearly indicated the pH sensitiveness and instability of micelles at lower pH. Taken together, a distinct release pattern in physiological and acidic conditions would be an invaluable approach in tumor drug delivery.

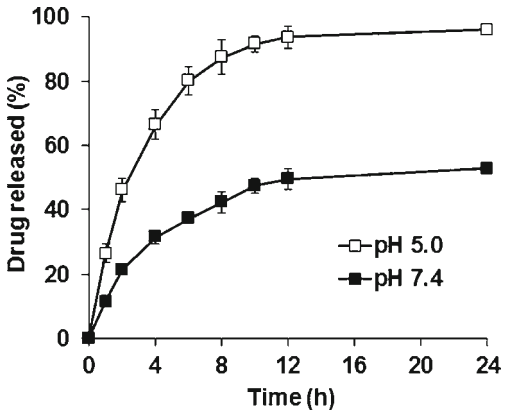


**Fig. 5** *In vitro* release profiles of IRI from IRI-BIC in physiological (pH 7.4) and acidic (pH 5.0) media at 37°C. Data are expressed as mean ± SD ($n = 3$).

### *In vitro* Cytotoxicity Study

The cytotoxic effect of free IRI and IRI-BIC was evaluated on SCC-7 breast cancer and A-549 non-small lung cancer cell lines (Fig. 6). In both cell lines, slightly more cells were inhibited with free IRI than with IRI-BIC in 24 h. Difference in efficacy might result from infusion of free drugs into the cell nucleus, while drug has to detach from drug-loaded micelles before diffusing into the nucleus [32]. The physicochemical properties of IRI-BIC such as size, drug loading, and release characteristics influence their growth inhibitory effect. In general, IRI interacts with Topoisomerase I–DNA complexes within the nucleus and has S-phase-specific cytotoxicity [33].

### Pharmacokinetic Study

The plasma concentration-time profiles of IRI and IRI-BIC following intravenous administration (5 mg/kg) are shown in Fig. 7. As expected, free IRI was readily cleared from the blood circulation within 4–6 h of drug administration and exhibited a linear pharmacokinetics [7]. This was in contrast to IRI-BIC, which remarkably prolonged the blood circulation time of drug throughout the duration of the study period. The corresponding parameters are shown in Table I. We observed significant differences between IRI and IRI-BIC for most of the pharmacokinetic parameters. For example,

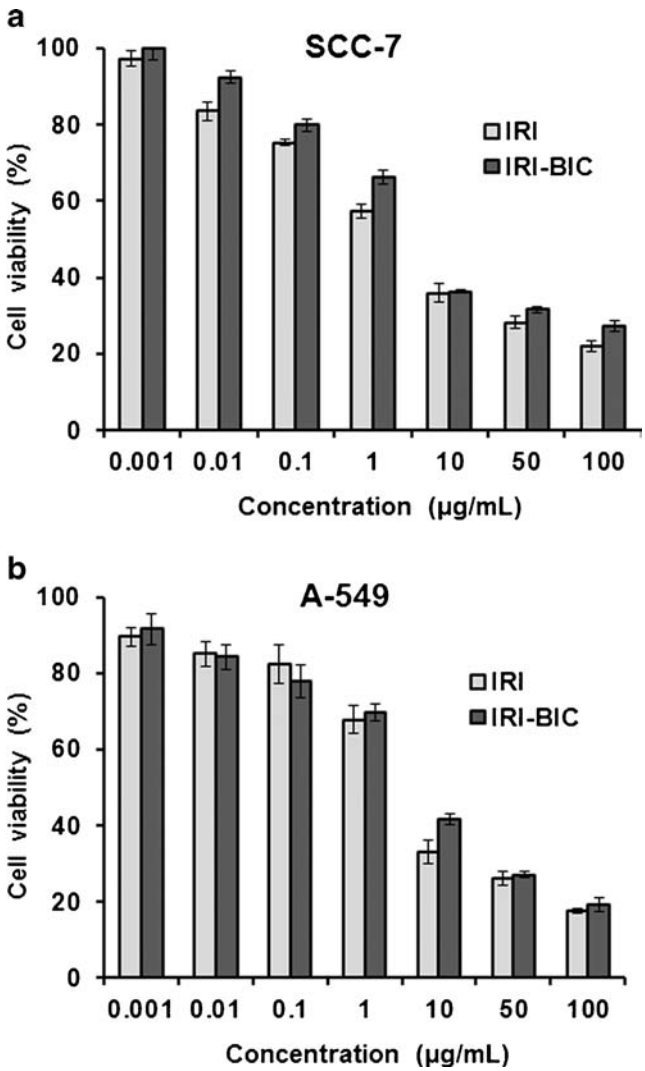


**Fig. 6** *In vitro* cytotoxicity of free IRI and IRI-BIC after 24 h exposure in (A) SCC-7 and (B) A-549 cells. Each value represents mean ± SD ($n = 4$).

IRI-BIC micelle showed five times lower $K_{el}$ compared to free IRI and similarly showed five times lower clearance than the free drug. IRI-BIC caused remarkable elevation of the total

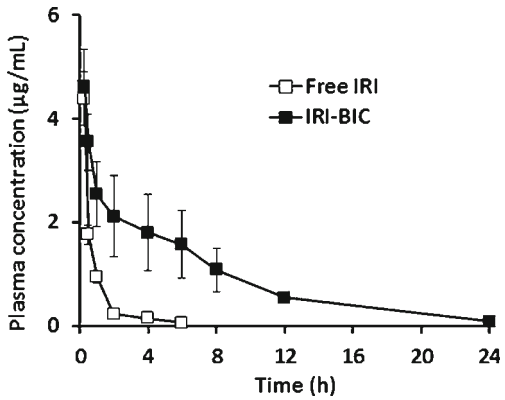


**Fig. 7** Plasma concentration-time profiles of free IRI and IRI-BIC following intravenous administration of a single dose of respective formulations. Each value represents a mean ± SD ($n = 3$).

**Table I** Pharmacokinetic Parameters of IRI after IV Administration of Free IRI and IRI-BIC to Rats

| | Free IRI | IRI-BIC |
|---|---|---|
| $K_{el}$ | 0.67 ± 0.01 | 0.12 ± 0.01 |
| $t_{1/2}$ | 1.04 ± 0.01 | 5.77 ± 0.53 |
| $AUC_{all}$ | 4.31 ± 0.73 | 25.54 ± 8.68 |
| $AUC_{INF}$ | 4.40 ± 0.75 | 27.32 ± 9.49 |
| Cl | 230.6 ± 39.5 | 40.5 ± 17.1 |
| $MRT_{last}$ | 0.76 ± 0.05 | 6.59 ± 0.34 |

Data are expressed as mean ± standard deviation ($n = 3$ per treatment)

plasma concentration and circulation time was notably higher compared to free drug. The overall AUC, which is representative of the presence of drug in the body, is manifold higher for IRI encapsulated in micelles. The micelles (5.77 ± 0.53 h) significantly increased the half-life ($t_{1/2}$) of drug compared with free drug injection (1.079 ± 0.07 h). Notably, mean retention time (MRT) was 7–8 folds higher compared with the free drug.

The enhanced *in vivo* performance of BIC micelles can be attributed to several factors. First, nano-sized particles with uniform size distribution were helpful in avoidance of rapid uptake by the reticuloendothelial system (RES) components [34]. Second, sustained release profile of micelles prolonged the presence of drug in the central compartment [35]. Third, presence of PEG reportedly enhances the shielding effect by virtue of conformational mobility to the particle; thereby complement system would be poorly activated *via* resisting phagocytosis. This will further prolong the blood circulation by minimizing recognition of micelles by the RES system and thereby decreasing the clearance rate of the drug [36, 37]. These results were consistent with previously published data, where a manifold increase in the plasma concentrations was observed after PEGylation [38]. It is important to note that BIC micelles, an electrostatically assembled carrier maintained its good stability in the physiological environment without becoming disassembled.

### *In vivo* Anti-Tumor Study

Encouraged by the pharmacokinetic and physicochemical data, we further examined the efficacy of a micellar carrier in tumor bearing mice. The anti-tumor efficacy of free IRI and IRI-BIC were studied in SCC-7 tumor bearing BALB/c nude mice. The respective formulations (at a dose of 5 mg/kg) were given on days 1, 4, 7 and 11, and the anti-tumor efficacy was calculated from the reduction in the ratio of tumor volume increase. As shown in Fig. 8a, the tumor volume

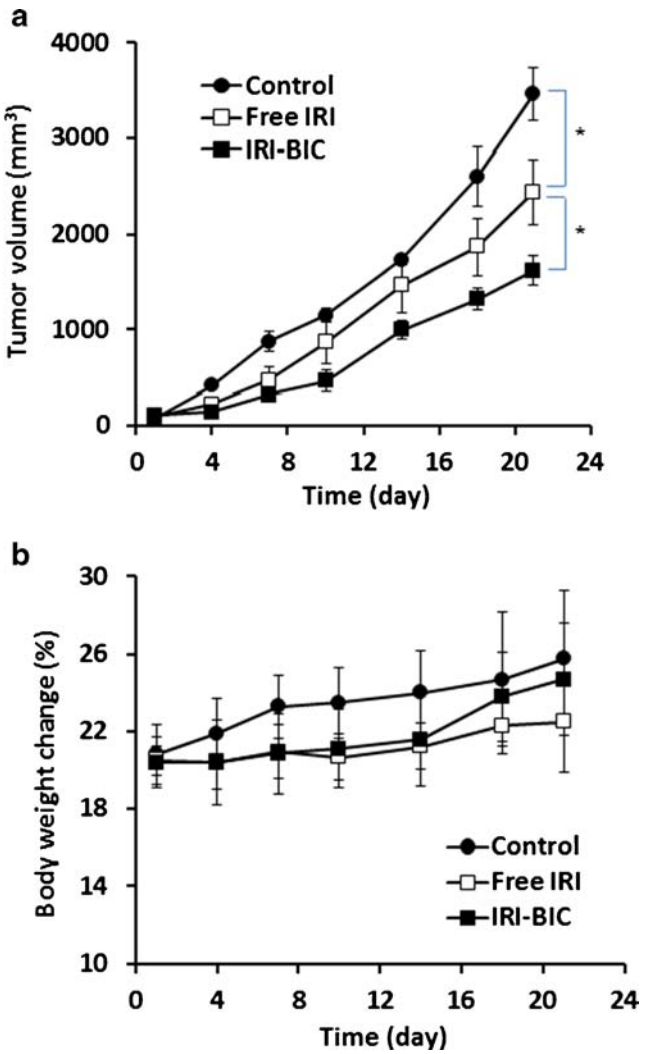


**Fig. 8** Anti-tumor efficacy of free IRI and IRI-BIC against SCC-7 xenograft tumor mice model. (**a**) Tumor volume and (**b**) body weight change. Each value represents a mean ± SD ($n = 6$).

showed a rapid increase in the untreated control group, however, tumor was significantly suppressed in drug-treated groups ($P<0.05$). Specifically, IRI-BIC caused remarkable inhibition of the growth of tumor compared to both untreated and IRI-treated groups. This effect can be explained by the poor pharmacokinetic profile of free IRI, which was rapidly cleared from the blood circulation with a smaller half-life compared to IRI-BIC [7, 38]. Consistent with the tumor volume, the effective tumor mass of BIC groups was significantly lower and different from that of the control and IRI-treated groups. The enhanced tumor regression from the BIC group might result from the longer circulation half-life ($t_{1/2}$) and lower elimination rate constant of drug. The high plasma concentration might augment the intracellular accumulation of drug at the cancer sites *via* EPR effect, subsequently permitting the potential action [39]. Furthermore, nanosize characteristics, core-shell architecture, sustained release in neutral pH, pH-dependent release in tumor pH, and presence of a micellar system could also confer enhanced uptake in cancer cells and thereby high tumor regression [40]. Change in body weight is an indicator of toxicity profile of drug or formulations. None of the formulations showed any concomitant overt signs of acute toxicity (Fig. 8b). Specifically, the IRI-BIC treated group maintained their body weights throughout. In the case of IRI-BIC, the drug was released in a sustained manner such that it did not surpass the therapeutic safe level and was gradually taken up by cancer cells in a time dependent manner. The results further indicate that IRI at a dose of 5 mg/kg is well-tolerated and does not show any drug-related toxicity. This is a significant observation, knowing that IRI produces a severe myelosuppresive effect and gastrointestinal toxicity.

## CONCLUSION

In summary, IRI-loaded pH sensitive BIC micelles with high payload capacity were successfully prepared *via* electrostatic immobilization. The BIC micelles were a nanosized (~50 nm) with uniform size distribution pattern (PDI~0.1). The obtained micelles exhibited pH-sensitivity with limited release in physiological conditions and significantly enhanced the release rate in acidic conditions, making it an ideal delivery system for tumor targeting. Results of pharmacokinetic studies showed an enhanced blood circulation time for BIC micelles, while free IRI was rapidly eliminated from the circulation pathway. The micelles markedly enhanced the plasma level of IRI with overall AUC higher than that of free drug. In addition, BIC showed a remarkable tumor regression profile in comparison with other groups, suggesting its high therapeutic efficacy. Therefore, we believe that IRI-loaded BIC micelles are a promising and exciting delivery system, which holds great potential in systemic cancer targeting.

## ACKNOWLEDGMENTS AND DISCLOSURES

This research was supported by a National Research Foundation of Korea (NRF) grant funded by the Ministry of Education, Science and Technology (No. 2012R1A2A2A02044997 and No.2012R1A1A1039059).

## REFERENCES

1. Kunii R, Onishi H, Machida Y. Preparation and antitumor characteristics of PLA/(PEG-PPG-PEG) nanoparticles loaded with camptothecin. Eur J Pharm Biopharm. 2007;67:9–17.
2. Zhang JA, Xuan T, Parmar M, Ma L, Ugwu S, Ali S, *et al.* Development and characterization of a novel liposome-based formulation of SN-38. Int J Pharm. 2004;270:93–107.

3. Ebrahimnejad P, Dinarvand R, Sajadi A, Jaafari MR, Nomani AR, Azizi E, *et al.* Preparation and in vitro evaluation of actively targetable nanoparticles for SN-38 delivery against HT-29 cell lines. Nanomedine Nanotechnol Biol Med. 2010;6:478–85.
4. Zhang H, Wang J, Mao W, Huang J, Wu X, She Y, *et al.* Novel SN38 conjugate-forming nanoparticles as anticancer prodrug: In vitro and in vivo studies. J Control Release. 2013;166:147–58.
5. Tobin P, Rivory L, Clarke S. Inhibition of acetylcholinesterase in patients receiving irinotecan (camptothecin-11). Clin Pharmacol Ther. 2004;76:505–6.
6. Bleiberg H. CPT-11 in gastrointestinal cancer. Eur J Cancer. 1999;35:371–9.
7. Zhang L, Cao DY, Wang J, Xiang B, Dun JN, Fang Y, *et al.* PEG coated irinotecan cationic liposomes improve the therapeutic efficacy of breast cancer in animals. Eur Rev Med Pharmacol Sci. 2013;17: 3347–61.
8. Guo S, Zhang X, Gan L, Zhu C, Gan Y. Effect of poly (ethylene oxide)-poly (propylene oxide)-poly (ethylene oxide) micelles on pharmacokinetics and intestinal toxicity of irinotecan hydrochloride: potential involvement of breast cancer resistance protein (ABCG2). J Pharm Pharmacol. 2010;62:973–84.
9. Matsumura Y. Preclinical and clinical studies of NK012, an SN-38-incorporating polymeric micelles, which is designed based on EPR effect. Adv Drug Deliv Rev. 2011;63:184–92.
10. Sapra P, Zhao H, Mehlig M, Malaby J, Kraft P, Longley C, *et al.* Novel delivery of SN38 markedly inhibits tumor growth in xenografts, including a camptothecin-11—refractory model. Clin Cancer Res. 2008;14:1888–96.
11. Kim JO, Ramasamy T, Yong CS, Nukolova NV, Bronich TK, Kabanov AV. Cross-linked polymeric micelles based on block ionomer complexes. Mendeleev Commun. 2013;23:179–86.
12. Mishra D, Kang HC, Bae YH. Reconstitutable charged polymeric (PLGA)(2)-b-PEI micelle for gene therapeutics delivery. Biomaterials. 2011;32:3845–54.
13. Riess G. Micellization of block copolymers. Prog Polym Sci. 2003;28: 1107–70.
14. Maeda H. The enhanced permeability and retention (EPR) effect in tumor vasculature: the key role of tumor-selective macromolecular drug targeting. Adv Enzyme Regul. 2001;41:189–207.
15. Yokoyama M, Okano T, Sakurai Y, Fukushima S, Okamoto K, Kataoka K. Selective delivery of adriamycin to a solid tumor using a polymeric micelle carrier system. J Drug Target. 1997;7:171–86.
16. Alakhov VY, Klinkski E, Li S, Pietrzynski G, Venne A, Batrakova E, *et al.* Block copolymer-based formulation of doxorubicin. From cell screen to clinical trials. Colloid Surf B Biointerfaces. 1999;16:113–34.
17. Kim JO, Kabanov AV, Bronich TK. Polymer micelles with cross-linked polyanion core for delivery of a cationic drug doxorubicin. J Control Release. 2009;138:197–204.
18. Bronich TK, Popov AM, Eisenberg A, Kabanov VA, Kabanov AV. Effects of block length and structure of surfactant on self-assembly and solution behavior of block ionomer complexes. Langmuir. 2000;16:481–9.
19. Oh KT, Bromberg L, Hatton TA, Kabanov AV. Block ionomer complexes as prospective nanocontainers for drug delivery. J Control Release. 2006;115:9–17.
20. Tian Y, Bromberg L, Lin SN, Hatton TA, Tam KC. Complexation and release of doxorubicin from its complexes with Pluronic P85-b-poly(acrylic acid) block copolymers. J Control Release. 2007;121: 137–45.
21. Tian Y, Ravi P, Bromberg L, Hatton TA, Tam KC. Synthesis and aggregation behavior of Pluronic F87/poly(-acrylic acid) block copolymer in the presence of doxorubicin. Langmuir. 2007;23:2638–46.
22. Ramasamy T, Kim J, Choi HG, Yong CS, Kim JO. Novel dual drug-loaded block ionomer complex micelles for enhancing the efficacy of chemotherapy treatments. J Biomed Nanotechnol. 2014;10: 1304–12.
23. Ramasamy T, Khandasami US, Ruttala H, Shanmugam S. Development of solid lipid nanoparticles enriched hydrogels for topical delivery of anti-fungal agent. Macromol Res. 2012;20:682–92.
24. Ramasamy TG, Haidar ZS. Characterization and cytocompatibility eval-uation of novel core–shell solid lipid nanoparticles for the controlled and tunable delivery of a model protein. J Bionanosci. 2012;5: 143–54.
25. Silverstein RM, Bassler GC, Morrill TC. Spectrometric Identification of Organic Compounds. 5th ed. NY: John Wiley & Sons; 1991. p. 91–142.
26. Shu S, Zhang X, Teng D, Wang Z, Li C. Polyelectrolyte nanoparticles based on water-soluble chitosan–poly(L-aspartic acid)–polyethylene glycol for controlled protein release. Carbohydr Res. 2009;344: 1197–204.
27. Blume A, Hubner W, Messner G. Fourier transform infrared spectroscopy of $^{13}C=O$-labeled phospholipids hydrogen bonding to carbonyl groups. Biochemist. 1988;27:8239–49.
28. Dicko A, Tardi P, Xie X, Mayer L. Role of copper gluconate/ triethanolamine in irinotecan encapsulation inside the liposomes. Int J Pharm. 2007;337:219–28.
29. Ramasamy T, Tran TH, Choi JY, Cho HJ, Kim JH, Yong CS, *et al.* Layer-by-layer coated lipid–polymer hybrid nanoparticles designed for use in anticancer drug delivery. Carbohydr Polym. 2014;102: 653–61.
30. Torchilin VP. PEG-based micelles as carriers of contrast agent for different imaging modalities. Adv Drug Deliv Rev. 2002;54:235–52.
31. Subedi RK, Kang KW, Choi HK. Preparation and characterization of solid lipid nanoparticles loaded with doxorubicin. Eur J Pharm Sci. 2009;37:508–13.
32. Ramasamy T, Tran TH, Cho HJ, Kim JH, Kim Y, Jeon JY, *et al.* Chitosan-based polyelectrolyte complexes as potential nanoparticulate carriers: physicochemical and biological characterization. Pharm Res. 2014;31:1302–14.
33. Liu LF, Desai SD, Li TK, Mao Y, Sun M, Sim SP. Mechanism of action of camptothecin. Ann NY Acad Sci. 2000;922:1–10.
34. Zhu S, Hong M, Tang G, Qian L, Lin J, Jiang Y, *et al.* Partly PEGylated polyamidoamine dendrimer for tumor-selective targeting of doxorubicin: The effects of PEGylation degree and drug conjugation style. Biomaterials. 2010;31:1360–71.
35. Assumpçao JU, Campos ML, Ferraz Nogueira Filho MA, Pestana KC, Baldan HM, FormarizPilon TP, *et al.* Biocompatible microemulsion modifies the pharmacokinetic profile and cardiotoxicity of doxorubicin. J Pharm Sci. 2013;102:289–96.
36. Lee Y, Lee H, Kim YB, Kim J, Hyeon T, Park H, *et al.* Bioinspired surface immobilization of hyaluronic acid on monodisperse magnetite nanocrystals for targeted cancer imaging. Adv Mat. 2009;20: 4154–7.
37. Parveen S, Sahoo SK. Long circulating chitosan/PEG blended PLGA nanoparticle for tumor drug delivery. Eur J Pharmacol. 2011;670:372–83.
38. Kim JY, Kim JK, Park JS, Byun Y, Kim CK. The use of PEGylated liposomes to prolong circulation life-times of tissue plasminogen activator. Biomaterials. 2009;30:5751–6.
39. Kim JH, Kim YS, Park K, Lee S, Nam HY, Min KH, *et al.* Antitumor efficacy of cisplatin-loaded glycol chitosan nanoparticles in tumor-bearing mice. J Control Release. 2008;127:41–9.
40. Mendoza AEH, Préat V, Mollinedo F, Blanco-Prieto MJ. In vitro and in vivo efficacy of edelfosine-loaded lipid nanoparticles against glioma. J Control Release. 2011;156:421–6.